## POLARIZATION OBSERVABLES IN $\vec{p}p \rightarrow pK^+\vec{Y}$ REACTIONS AT 2.9 GeV

F. Balestra, S. Bossolasco, M.P. Bussa, L. Fava, L. Ferrero, R. Garfagnini, A. Grasso, A. Maggiora, D. Panzieri, G. Piragino, F. Tosello, and G. Zosi
*Istituto di Fisica "A. Avogadro" and INFN, Torino, Italy*

L.C. Bland, T.W. Bowyer, S. Choi, W.W. Jacobs, Y. Kim, and S.E. Vigdor
*Indiana University Cyclotron Facility, Bloomington, Indiana 47408*

J. Arvieux, Y. Bedfer, R. Bertini, F. Brochard, and J.C. Faivre
*Laboratoire National Saturne, Saclay, France*

I.V. Falomkin, V.I. Lyascenko, G.B. Pontecorvo, V. Serdyuk, V.I. Travkin, and B. Zalikanov
*Joint Institute for Nuclear Research, Dubna, Russia*

As outlined in Ref. 1, the DISTO (Dubna-Indiana-Saclay-Torino) collaboration is preparing for an approved experiment at the Saturne synchrotron in Saclay to measure polarization observables in kinematically complete studies of hyperon production. These first *exclusive* polarization measurements should help to pin down the mechanism for producing strangeness in proton-induced reactions within the meson-exchange regime, and may lead the way to analogous coincidence experiments at higher energies to investigate the evolution of the mechanism toward the quark-gluon regime. Indeed, we have argued[2] on general grounds that the normal polarization transfer coefficient $D_{NN}$, in particular, will be very sensitive to the relative contributions from different diagrams in both meson-exchange and parton recombination[3] models of the interaction. Our planned simultaneous measurement of $D_{NN}$ for $\vec{\Lambda}^0$ and $\vec{\Sigma}^0$ production provides an especially strong constraint on the models.

The DISTO apparatus is designed to track simultaneously through a strong magnetic field the four charged products from $\Lambda^0$ production: $\vec{p}p \rightarrow pK^+\vec{\Lambda}^0 \rightarrow pK^+p\pi^-$. It thereby also enables kinematically complete measurements for $\vec{\Sigma}^0$ production, where we will miss only the photon from the (100% branching ratio) $\Sigma^0 \rightarrow \Lambda^0 + \gamma$ decay. The hardware (Level 1) trigger will select events with at least four charged prongs within the detector acceptance, while a software (Level 2) trigger will search for the spatial separation between reaction and decay vertices that is characteristic of the weak ($\tau \sim 10^{-10}$ s) $\Lambda^0$ decay. The particle momenta will be determined with sufficient resolution to separate $\Lambda^0$ from $\Sigma^0$ production in the missing mass spectrum reconstructed from the p and $K^+$ momenta at the reaction vertex. The tracking detectors will comprise two scintillating fiber chambers embedded in the field (each with 3 planes of 1-mm square fibers, providing $y$, $u$, and $v$ position information) and two $x-u-v$ multiwire proportional chambers at the edge of the magnet.

Behind these detectors (at a radial distance of $\simeq$140 cm from the target) will be placed a plastic scintillator hodoscope being designed and built at IUCF.[1] All the detectors will have cylindrical geometry centered about the liquid hydrogen target to be placed at the center of the (approximately) cylindrically symmetric field.

Substantial progress has been made during the past year on all of the technical issues relevant to mounting production runs in 1994. We concentrate here mainly on the developments made at IUCF: the fabrication of the first elements of the scintillator hodoscope and beam tests of their response; extensive simulations of the detector acceptance, resolution, and achievable polarization precision; the design of a trigger for a small sample of p-p elastic scattering events to monitor detector performance and beam polarization; and further developments of the software for the Level 2 trigger and for the full reconstruction of hyperon production events. After describing this work, we will summarize briefly the major advances made by other groups in the collaboration.

The IUCF hodoscope will consist of two left-right symmetric arms, each comprising 6 long horizontal elements curved along the surface of a cylinder (to provide crude information on the vertical $y$-coordinate of detected particles) and 10 straight vertical elements (to measure $x$). The hodoscope will provide a fast multiplicity trigger for the experiment, in combination with the scintillating fiber chambers. It will also provide the only means we have of distinguishing the identification of the proton vs. kaon from the primary reaction vertex, a distinction that is essential for correctly reconstructing the missing mass. The identification of p and $K^+$ (both of which are minimum-ionizing over most of phase space) is based on their relative arrival times at the hodoscope, in combination with the measured momenta of the corresponding tracks. As shown by simulations in Fig. 1, the time resolution between pairs of hodoscope hits must be $\leq$1.0 ns FWHM to accomplish this identification reliably. The timing of hits at the hodoscope will also serve to confirm the matching of horizontal and vertical track information suggested by the other chambers. As outlined below, the hodoscope will also play a central role in defining a hardware trigger for p-p scattering monitor events.

Budget restrictions have dictated cost savings on the hodoscope, effected by using phototubes on one end only of each element and leading-edge, rather than constant-fraction, discriminators. This approach necessitates calibrations and correction in software for variations of the timing of each scintillator with signal pulse height and with distance from the phototube, as well as position-dependent energy corrections associated with light attenuation. To facilitate *in-situ* calibrations, we have built into the hodoscope layout small overlap regions (subtending 0.2° lab angle at the target) between adjacent $x$-elements, which are to be located alternately in front of and behind the $y$-elements, with phototubes alternating between the bottom and top ends. (The degree of overlap must be kept small to avoid excessive complication of the particle multiplicity trigger.) Particles falling within such an overlap region have very well-defined position, including redundant information on $y$ from the time difference between the two adjacent $x$-element phototube signals. Much of the needed calibration will be based on the two $x$-element and one $y$-element times and pulse heights recorded for these overlap-region particles.

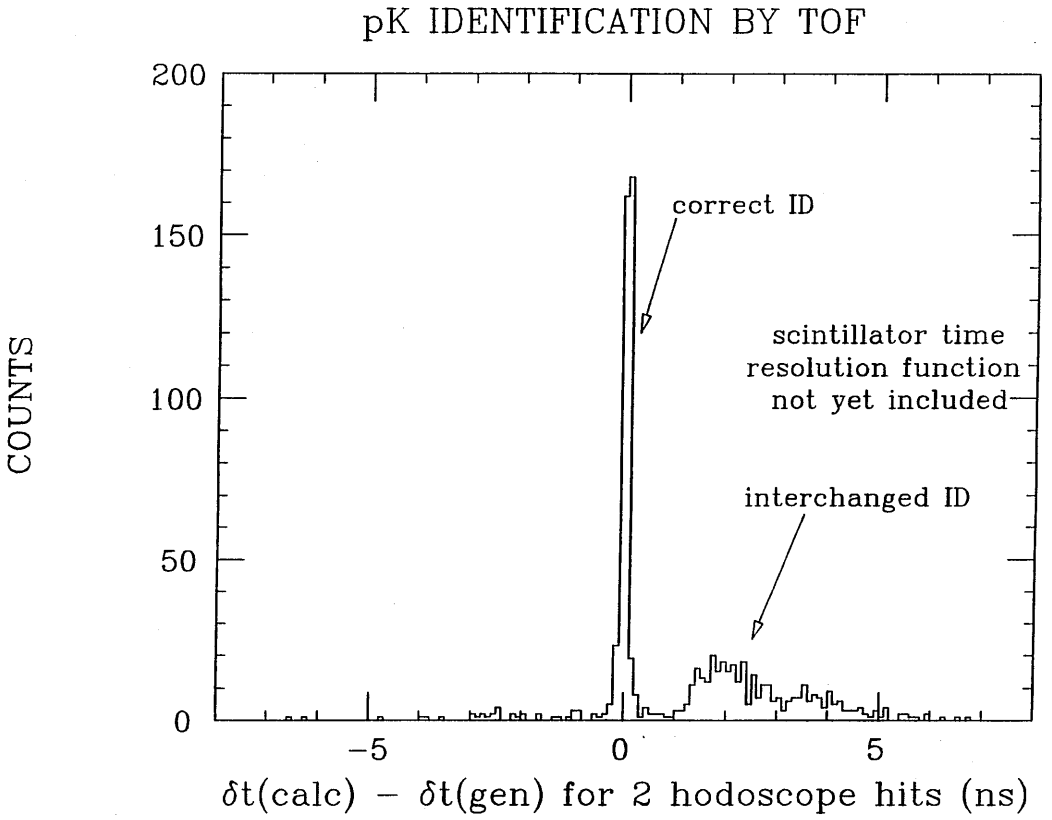


*Figure 1.* Simulation results for pp $\rightarrow$ pK$^+\Lambda$, indicating how the p and K$^+$ products can be distinguished via their relative time of flight $\delta t$ from the primary reaction vertex to the hodoscope. $\delta t$(calc) is the expected flight time difference for a given assumed assignment of the two particle types to the two reconstructed tracks, based on the reconstructed momenta and track lengths. The spectrum is incremented twice for each reconstructed event, once for each possible p vs. K$^+$ assignment. The GEANT-generated time difference $\delta t$(gen) is reproduced only for the correct particle identification. The width of the observed peak reflects the resolution in reconstructing the particle momenta and track lengths, but does not yet have the scintillator time resolution folded in.

The scintillator responses and calibration schemes were tested in April 1993 for the first six (3 $x$ and 3 $y$) hodoscope elements fabricated. The test was carried out at IUCF with split beam, by detecting p-p elastic scattering events induced on a $CH_2$ target by 200-MeV protons. A small scintillator close to the target was used to detect the protons scattered to one side of the beam, while the prototype hodoscope was used in coincidence on the other side. The 6 elements were arranged just as they would be within a final hodoscope arm, with the $x$-elements fixed to span the lab angle range from 31° to 46°, and the $y$-elements set in various locations during the run, to cover the entire relevant range of

distances from the $x - y$ overlap regions to the respective phototubes. In this test run we used *both* leading-edge and constant-fraction discriminators on each hodoscope element, in order to calibrate the corrections for time walk.

Figure 2 shows typical spectra acquired for elastically scattered protons falling in the narrow adjacent-$x$ overlap regions, and thus giving triple coincidences ($x_2 \cdot x_{(1\ or\ 3)} \cdot y_i$) among hodoscope elements. These raw data clearly illustrate the variation of times and pulse heights with distances from the phototubes (superimposed on p-p scattering kinematic variations). The data from the test run are currently being analyzed to refine the various calibration algorithms and to optimize the software corrections. The analysis to date shows that we will be able to meet our goal of FWHM $\leq$1.0 ns resolution on the relative corrected times from pairs of hodoscope elements. In the wake of the successful test run, the rest of the hodoscope elements are currently being fabricated. The entire detector should be completed in Fall, 1993.

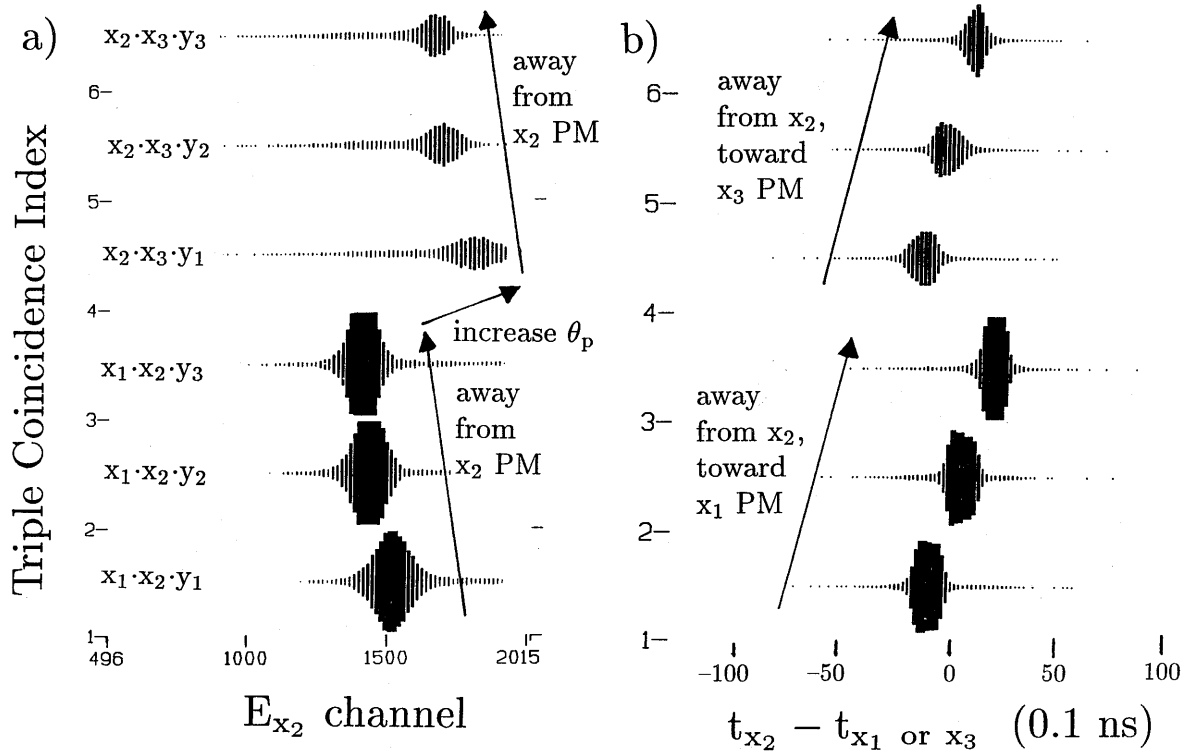


*Figure 2.* On-line spectra from the hodoscope test run, showing the distribution of triple coincidence events with respect to (a) the signal pulse height in the middle $x$ element and (b) the arrival time difference between the phototube signals for the middle $x$ and adjacent $x$ elements. The six groups in each frame represent the six different triple-coincidence pixels, as indicated by the labels. The variations observed arise in part from the changing distance from the $x$-element phototubes, and in part from p-p scattering kinematics.

We have also continued our detailed computer simulations of the whole experiment, utilizing the CERN package GEANT in combination with our own event reconstruction software HYPPO. A major question addressed by simulations during the past year was the quantitative assessment of potential benefits from expanding the vertical acceptance of the detectors to $\pm 21.0°$ (the maximum allowed by the pole gap of the magnet to be used). Critical components of this assessment dealt with the effects of the vertical acceptance on the phase space coverage and on the statistical precision attainable for $\Lambda^0$ and $\Sigma^0$ polarization measurements. We found that none of the improvements were sufficient to justify the extra cost (mainly for additional electronic readout channels) that would be required by the expansion. The clear gain in solid angle is unimportant because we already expect our counting rates to be limited by the capabilities of the front-end electronics.

Figure 3 shows simulated event distributions relevant to the determination of normal [parallel to $\hat{n} \equiv (\vec{k}_{inc} \times \vec{k}_Y)/|\vec{k}_{inc} \times \vec{k}_Y|$] component $\Lambda^0$ and $\Sigma^0$ polarizations, for the chosen vertical detector acceptance of $\pm 15.5°$. For the weak $\Lambda^0$ decay, this polarization is extracted from the (parity-violating) asymmetry of the decay protons in emission angle

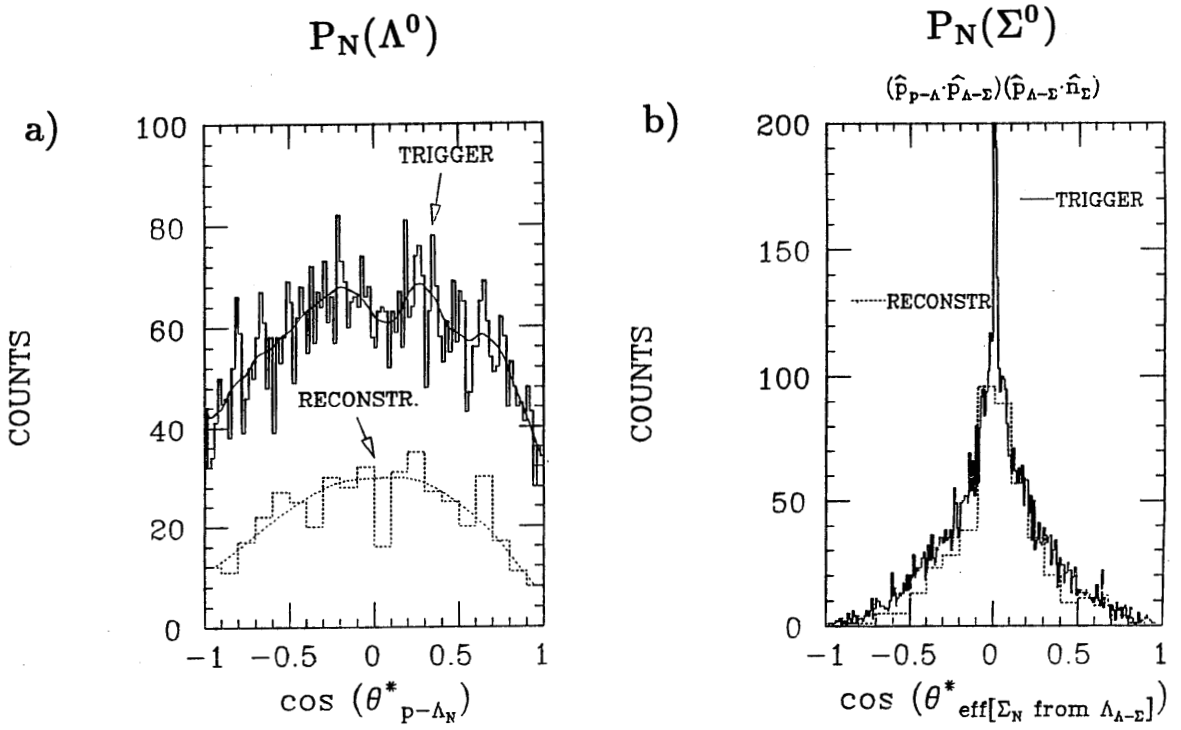


*Figure 3.* The distributions of generated and reconstructed events from a pp $\rightarrow$ pK$^+\Sigma^0$ simulation, relevant to the extraction of the normal polarization component for the (a) daughter $\Lambda^0$ and (b) parent $\Sigma^0$. The distributions reveal no instrumental asymmetries within statistics, and allow us to deduce the figures of merit for the two polarization determinations. The curves in (a) represent smoothed versions of the histograms. See text for details.

$\theta^*$ with respect to $\hat{n}$ in the $\Lambda^0$ rest frame. In Fig. 3(a) the distribution of the simulated (unpolarized) $\Lambda^0$ decays is shown with respect to $\cos\theta^*$ for both the generated value of $\theta^*$ (for all events that would pass the Level 1 trigger) and the reconstructed value of $\theta^*$. (Only a fraction of the generated events is successfully reconstructed because the present version of HYPPO analyzes only those events with the simplest topology: p and $K^+$ tracks completely on one side of the beam, $\Lambda^0$ decay products completely on the other.) Both distributions reveal zero instrumental asymmetry within the statistical precision of the simulation, although the acceptance for $\Lambda^0$ decays is clearly not *isotropic* in the $\Lambda^0$ rest frame. The acceptance would be more nearly isotropic with the expanded vertical detector coverage, but the gain in figure of merit for the $\Lambda^0$ polarization measurement would be only ~6%. The figure of merit has been extracted from the simulations assuming that we analyze the data by determining $P_\Lambda$ from an error-weighted average of the independent results $P_{\Lambda_i}$ obtained for various non-overlapping bins in $x \equiv |\cos\theta^*|$:

$$P_{\Lambda_i} = \frac{1}{\alpha x_i}\left[\frac{N(+x_i) - N(-x_i)}{N(+x_i) + N(-x_i)}\right], \tag{1}$$

where $N$ represents the number of events observed in the bin of interest and $\alpha = 0.642 \pm 0.013$ is the known $\Lambda^0$ decay asymmetry parameter. This analysis method assumes no instrumental asymmetry, but requires no other knowledge of the shape of the acceptance function.

The extraction of $\Sigma^0$ polarization is more complicated because we again measure the $\Lambda^0$ polarization, but the polarization transfer in the electromagnetic decay $\vec{\Sigma}^0 \to \vec{\Lambda}^0 + \gamma$ depends on the $\Lambda$'s emission direction ($\hat{p}_{\Lambda-\Sigma}$) in the $\Sigma^0$ rest frame:[4]

$$\vec{P}_\Lambda = -(\vec{P}_\Sigma \cdot \hat{p}_{\Lambda-\Sigma})\hat{p}_{\Lambda-\Sigma}. \tag{2}$$

Thus, the relevant distribution of events is with respect to the *product of two independent* $\cos\theta^*$ factors, one describing the $\Lambda$'s emission in the $\Sigma^0$ rest frame and the other the proton's emission in the $\Lambda^0$ rest frame. As shown in Fig. 3(b), the acceptance is sharply peaked around zero for this product. (The broader peak for reconstructed events reflects primarily the simulated resolution in reconstructing the $\Sigma^0$ rest frame.) Nonetheless, the tails of this distribution (which again reveal no instrumental asymmetry) allow a reasonable measurement of $P_\Sigma$. On the basis of the simulations we estimate that the following statistical precisions can be attained in *one day* of running, within each of 10 equally populated bins (e.g., subdividing the full range in transverse momentum transfer $p_T$): $\pm 0.030$ for the normal component of $\Lambda^0$ polarization in $pp \to pK^+\vec{\Lambda}^0$; $\pm 0.097$ ($\pm 0.064$) for the normal (sideways) component of $\Sigma^0$ polarization in $pp \to pK^+\vec{\Sigma}^0$. The extraction of *other* components of the $\Lambda^0$ and $\Sigma^0$ polarization vectors from the experiment will rely on calibrating the substantial instrumental asymmetries expected and observed for those cases.

It is possible to monitor the incident beam polarization continuously in the DISTO experiment itself by analyzing $\vec{p}$-p elastic scattering events as well as the hyperon production events. Although there are no existing $\vec{p}$-p scattering data at 2.9 GeV, the systematics of measurements at lower and higher energies[5] indicate a probable broad positive peak in the analyzing power ($A_y \simeq +0.2$) centered about a momentum transfer $t = -1.7$ (GeV/c)$^2$.

Coincidences from the corresponding events can be detected in the DISTO setup with the forward proton (at $\theta_{lab} \simeq 20$–$30°$) on either the left or right detector arms. We have designed a selective hardware trigger for the events of interest, requiring one of the protons to fall within one of the narrow overlap regions between adjacent hodoscope $x$-elements, in order to keep the trigger rate manageable. A fast memory lookup unit will be used to select only those left–right hodoscope element coincidences appropriate to elastic scattering. The events passing this trigger will be recorded on scalers for every beam spill, and will be written to event tape for selected spills. The p-p events are expected as well to be very useful for detector calibrations and diagnostics.

In parallel with the above work, we have continued to develop the software for the Level 2 trigger and for the event reconstruction for hyperon production events. The Level 2 trigger is based on the spatial separation between reaction and $\Lambda$ decay vertices. The degree of inconsistency of the recorded tracks with a common vertex can be determined rapidly from the measured *vertical* positions, which (unlike the horizontal positions) vary nearly linearly with detector distance within each track. Our work on the Level 2 trigger during the past year has concentrated on ways to extend the algorithm to deal more effectively with ambiguous events that are plagued by missing or extra hits. The major work on the reconstruction software has been aimed at expanding the range of event topologies analyzed, improving the algorithms for sorting hits from different chambers into self-consistent tracks, improving the speed of the vertex reconstruction, and reconstructing the variables relevant to $\Sigma^0$ polarization determinations.

Major advances have also been made during the past year on all the other equipment needed for the DISTO setup. The S170 magnet was delivered from CERN and installed at Saturne in summer 1992. Field maps and beam profile measurements were made during the fall and winter. The design of the small-diameter conical beam pipe (to be made from carbon fiber material) and liquid hydrogen target for the experiment are well under way. An electronics hut has been provided and cables between hut and cave are currently being installed. Prototype tests for the scintillating fiber and wire chambers are scheduled for July 1993. The scintillating fibers will be read out with Hamamatsu (model 4140-20) 16×16-anode PM tubes, which have <2% crosstalk between adjacent anodes, and PCOS III electronics. Design of the trigger electronics is completed and many of the necessary modules have now been purchased or fabricated. A preliminary version of the data acquisition system – based on storage of data in a fast VME memory buffer during beam spills, and subsequent processing by four RISC 5000 CPU's and a Silicon Graphics Iris workstation – has been implemented. This progress should enable production running during 1994. In addition, a new proposal has been submitted to Saturne (led by Dave Gill of TRIUMF) to use the DISTO equipment in a subsequent study of the OZI-rule-evading process[6] $pp \rightarrow pp\phi$ near threshold. That experiment will require the addition of water Cerenkov detectors to distinguish K's (from the decay $\phi \rightarrow K^+K^-$) from background pions, since the short-lived $\phi$ does not permit a Level 2 trigger based on separation of the reaction and decay vertices.

1. S. Bossolasco, *et al.*, IUCF Sci. and Tech. Report, 1992, p. 88; A. Maggiora, *et al.*, in *Proc. Intl. Workshop on Flavour and Spin in Hadronic and Electromagnetic Interactions*, (Italian Physical Society, Bologna, 1993) p. 111.
2. S.E. Vigdor, in *Proc. Intl. Workshop on Flavour and Spin in Hadronic and Electromagnetic Interactions*, (Italian Physical Society, Bologna, 1993) p. 317.
3. T. deGrand, J. Markkanen, and H.I. Miettinen, Phys. Rev. D **32**, 2445 (1985).
4. R. Gatto, Phys. Rev. **109**, 610 (1957).
5. F. Lehar, in *Proc. 7th Intl. Conf. on Polarization Phenomena in Nuclear Physics*, Colloque de Physique **51**, C6-19 (1990).
6. J. Ellis, E. Gabathuler, and M. Karliner, Phys. Lett. B **217**, 173 (1989).